Chemical Science

EDGE ARTICLE

View Article Online
View Journal | View Issue

CrossMark click for updates

Cite this: *Chem. Sci.*, 2015, **6**, 5511

A supramolecular nanovehicle toward systematic, targeted cancer and tumor therapy†

Ruizheng Liang,‡[a] Shusen You,‡[a] Lina Ma,[b] Chunyang Li,[a] Rui Tian,[a] Min Wei,*[a] Dan Yan,*[b] Meizhen Yin,*[a] Wantai Yang,[a] David G. Evans[a] and Xue Duan[a]

Received 19th March 2015
Accepted 22nd June 2015

DOI: 10.1039/c5sc00994d

www.rsc.org/chemicalscience

A supramolecular nanovehicle (denoted as SNV) was fabricated by encapsulating zinc phthalocyanine (ZnPc) and doxorubicin (DOX) into a copolymer (PVP-*b*-PAA-*g*-FA), so as to achieve systematic and synergistic chemotherapy-photodynamic therapy (PDT), targeted tumor imaging and therapy. The sophisticated copolymer designed in this work can load the PDT photosensitizer (ZnPc) and chemotherapy drug (DOX) simultaneously, which exhibits an excellent performance in chemotherapy-PDT targeted cancer and tumor therapy for both *in vitro* studies performed with HepG2 cells and *in vivo* tests with mice. This work provides a new drug formulation with a chemotherapy-PDT synergistic effect by virtue of the supramolecular material design, which possesses the advantages of an ultra-low drug dosage and highly-efficient *in vivo* targeted tumor imaging/therapy.

Open Access Article. Published on 22 Juni 2015. Downloaded on 28.01.2026 20:20:08.
This article is licensed under a Creative Commons Attribution-NonCommercial 3.0 Unported Licence.

Introduction

The social and economic burden of cancer demands a spectrum of therapeutic methodologies, which so far includes surgery, chemotherapy,[1,2] radiotherapy, hyperthermia[3] and photodynamic therapy (PDT).[4] However, owing to the limit of each individual therapeutic route, a single methodology is rarely sufficient to overcome cancers.[5–7] For instance, surgery suffers from a precise control over the resection of a tumor while chemotherapy and radiotherapy would inevitably cause damage to normal tissues when killing cancerous cells.[8] Recently, to overcome the limitation of a single therapy and to enhance/optimize the anticancer efficacy, the integration of multimodal treatment strategies for the purpose of achieving a synergistic or systematic therapy has attracted considerable research interest.[9–11]

PDT is a promising therapeutic modality owing to the advantages of being an effective and non-invasive treatment of diseased tissues with minimal side-effects. The principle of PDT involves the injection of a photosensitizer followed by visible-light irradiation to generate singlet oxygen that induces an effective destruction of diseased tissues.[12–18] In addition, fluorescence emission of the photosensitizers can be further employed for cancer fluorescence imaging.[19,20] The properties of the photosensitizer play a key role in determining the PDT effectiveness, which has been regarded as the research focus in this area. An ideal photosensitizer should possess the following properties: (1) a monomeric state with a high singlet oxygen quantum yield;[21–27] (2) a near-IR light response to allow remarkable tissue penetration to deep-seated cancer cells;[28–30] (3) a targeting ability and a suitable delivery vehicle toward tumors in terms of inhibiting the side effects on normal cells.[31–37]

In spite of the advantages of PDT mentioned above, its performance as an individual therapy is far from highly satisfactory. For instance, the limited tissue penetration of the light source makes the PDT effectiveness for internal tumors suboptimal.[38–40] From the viewpoint of a systematic therapy, the combination of PDT and chemotherapy for tumor therapy is a favorable strategy.[41] Chemotherapy is the treatment of cancer with chemotherapeutic drugs (CTDs) to restrain DNA and RNA synthesis and promote cell death, which has been one of the traditional modalities in current clinical applications.[42,43] The main obstacle of CTDs lies in the serious side effects on normal tissues due to their powerful and nonselective activity. Based on these considerations, the combination of PDT and chemotherapy by virtue of a biocompatible and targeted drug delivery vehicle is a highly desirable and systematic approach, utilising the advantages of both of these cancer therapies. Compared with each individual method, the combined chemotherapy-PDT would lead to a largely-enhanced therapeutic efficacy, decreased drug dosage and depressed side effects.

Herein we report a supramolecular nanovehicle (SNV) to achieve systematic and synergistic chemotherapy-PDT targeted

[a]*State Key Laboratory of Chemical Resource Engineering, Beijing Laboratory of Biomedical Materials, Beijing University of Chemical Technology, Beijing 100029, P. R. China. E-mail: weimin@mail.buct.edu.cn; yinmz@mail.buct.edu.cn; Fax: +86-10-64425385; Tel: +86-10-64412131*

[b]*Beijing Shijitan Hospital, Capital Medical University, Beijing 100038, P. R. China. E-mail: yd277@126.com*

† Electronic supplementary information (ESI) available: NMR spectra, ITC, UV-vis spectra, zeta potential, TEM and additional characterization data. See DOI: 10.1039/c5sc00994d

‡ These authors equally contributed to this work.

Open Access Article. Published on 22 Juni 2015. Downloaded on 28.01.2026 20:20:08.
This article is licensed under a Creative Commons Attribution-NonCommercial 3.0 Unported Licence.

cancer imaging and therapy, which involves a two-step approach: (i) the synthesis of a copolymer (folic acid chemically-modified polyvinylpyrrolidone-*b*-polyacrylic acid, denoted as PVP-*b*-PAA-*g*-FA) with a targeting capability toward cancer cells; (ii) the encapsulation of a PDT photosensitizer (zinc phthalocyanine, ZnPc) and a chemotherapy drug (doxorubicin, DOX) into the copolymer to obtain the final SNV micelle (denoted as ZnPc-DOX/SNV; Scheme 1). The copolymer PVP-*b*-PAA-*g*-FA plays the key role as a multifunctional SNV: the introduction of acidic DOX neutralizes the partially ionized FA and therefore constitutes the hydrophobic core of the micelle; the remaining ionized FA and terminal PVP (ZnPc is combined with PVP by hydrogen bonding interactions) serve as the exterior shell of the micelle. This achieves an amphiphilic supramolecular nanovehicle (SNV) with a targeted cancer therapy owing to the overexpression of FA toward cancer cells.[44–46] The sophisticated SNV designed in this work can load the PDT photosensitizer and chemotherapy drug simultaneously, which exhibits an excellent performance in chemotherapy-PDT targeted cancer and tumor therapy both *in vitro*, performed with HepG2 cells, and *in vivo* with mice. The synergistic effect of chemotherapy and PDT (ultra-low drug dosage, highly-efficient behavior and *in vivo* targeted tumor imaging and therapy) is the most distinct feature of the combined therapy in this work.

Experimental section

Materials

N-Vinylpyrrolidone (NVP, Alfa Aesar, 99%), *tert*-butyl acrylate (*t*BA, Alfa Aesar, 99%), *N*,*N*-dimethylformamide (DMF) and 2-butanone (Sinopharm, 99%) were purified by distillation under reduced pressure before use. The cyclic ligand 5,5,7,12,12,14-hexamethyl-1,4,8,11-tetra-azacyclo-tetradecane (Me_6Cyclam), was synthesized according to the method described by Hay and Lawrance.[47] CuCl and CuBr (Aldrich, 98%) were purified by stirring in acetic acid followed by washing with methanol before drying under vacuum. Ethyl 2-bromoisobutyrate (EBiB, Alfa Aesar, 99%), *N*,*N*-diisopropylethylamine (DIPEA, Aladdin, 99%), folic acid (FA, 99%) and 2-(7-aza-1*H*-benzotriazole-1-yl)-1,1,3,3-tetramethyluronium hexafluorophosphate (HATU, Aladdin, 99%) were used as received without further purification. Zinc phthalocyanine (ZnPc) was purchased from J&K (97%). The disodium salt of 9,10-anthracenedipropionic acid (APDA) was purchased from Sigma. Basic alumina and all other reagents were purchased from Sinopharm and used as received without further purification.

Dulbecco's modified eagle's medium (DMEM) containing high glucose, L-glutamine and sodium pyruvate, pen-strep (10 000 units per mL penicillin and 10 000 μg mL^{-1} streptomycin) and 0.25% trypsin–EDTA were purchased from Gibco (Invitrogen, Carlsbad, CA). Fetal bovine serum (FBS) was purchased from Hyclone (Thermo Scientific, Rockford, IL). Phosphate-buffered saline (PBS) was purchased from Solarbio Science & Technology Co, Ltd (Beijing, China). 3-(4,5-Dimethylthiazol-2-yl)-2,5-diphenyltetrazolium bromide (MTT) and potassium iodide (PI) were purchased from Sigma. Human liver carcinoma (HepG2) cells were obtained from the Institute of Basic Medical Sciences Chinese Academy of Medical Sciences and cultured in DMEM containing 10% (v/v) FBS and 1% pen-strep at 37 °C in a humidified atmosphere containing 5% CO_2.

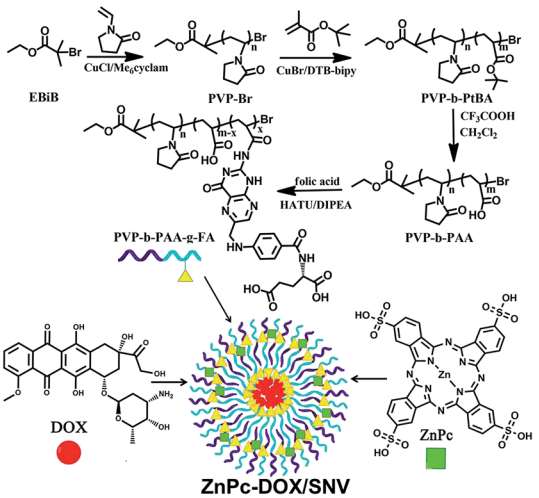

Scheme 1 The synthesis process of PVP-*b*-PAA-*g*-FA and a schematic illustration of the structure of ZnPc-DOX/SNV.

Preparation of ZnPc(*x*%)/SNV and ZnPc-DOX/SNV

ZnPc/SNV and ZnPc-DOX/SNV were prepared for the study of single PDT and chemotherapy-PDT, respectively. Firstly, the copolymer PVP-*b*-PAA-*g*-FA serving as a targeting drug delivery substrate was synthesized *via* chemical binding with FA to specifically over-express the HepG2 cells. The detailed synthesis procedure involves a three-step route and two intermediate products (PVP-Br and PVP-*b*-PAA), which is described in the ESI (Scheme S1†). Subsequently, a series of ZnPc(*x*%)/SNV materials were prepared by incorporation of ZnPc and PVP-*b*-PAA-*g*-FA through a facile liquid synthesis method. In brief, ZnPc and PVP-*b*-PAA-*g*-FA with various mass ratios (ZnPc : PVP-*b*-PAA-*g*-FA = 1 : 6; 1 : 12; 1 : 15; 1 : 18; 1 : 24, respectively) were simultaneously added into a centrifuge tube; each mixture was stirred at 25 °C to produce a homogeneous solution. For the preparation of ZnPc-DOX/SNV, muriatic DOX was added into the ZnPc(*x*%)/SNV solution, followed by a strong ultrasonic treatment for 0.5 h and then vigorous agitation for 12 h. Finally, the ZnPc-DOX/SNV micelles were purified by dialysis against pure water (molecular weight cut off 3500) to remove the unbound ZnPc and DOX. The reference samples, ZnPc(*x*%)/PVP-Br and ZnPc-DOX/PVP-Br, were prepared in a similar way by using the intermediate copolymer PVP-Br as the drug delivery substrate.

Detection of singlet oxygen

As a singlet oxygen sensor,[48] the disodium salt of 9,10-anthracenedipropionic acid (APDA) was used to detect the singlet oxygen generated from the ZnPc(*x*%)/SNV photosensitizer. Normally, an APDA solution (150 μL, 7.5 mM) was added into the ZnPc(*x*%)/SNV suspension (concentration: 10 μg mL^{-1}, 3 mL) and mixed thoroughly, followed by irradiation at 650 nm using a simulated sunlight source with an optical filter of 650 ±

 This journal is © The Royal Society of Chemistry 2015

Open Access Article. Published on 22 Juni 2015. Downloaded on 28.01.2026 20:20:08.
This article is licensed under a Creative Commons Attribution-NonCommercial 3.0 Unported Licence.

5 nm. The decrease rate of the UV absorption intensity at 378 nm is proportional to the amount of singlet oxygen produced, and the absorbance value was recorded per minute.

In vitro studies on cancer cells

HepG2 cells were cultured and expanded in a 25 cm^2 cell-culture flask. After reaching 80–90% confluence, the HepG2 cells were washed with PBS, and afterwards detached from the flask through the addition of 1.0 mL of 0.25% trypsin for 1–3 min at 37 °C. HepG2 cells (2×10^4 cells per well) were seeded into two 96-well plates. To study the chemotherapy-PDT performance, cells were treated with different concentrations of DOX, DOX/SNV, ZnPc, ZnPc/SNV, ZnPc-DOX/SNV and ZnPc-DOX/PVP-Br, respectively. After a further incubation of 24 h, the cells were washed with PBS 3 times. The plates were irradiated with a simulated sunlight source (optical filter: 650 ± 5 nm; power density: 10 mW cm^{-2}) for 30 min. The colorimetric MTT was used to determine the cell viability. To study the photo- and dark-toxicity effect, HepG2 cells (2×10^4 cells per well) were seeded into two 96-well plates and then treated with DOX (5 μg mL^{-1}), ZnPc (5 μg mL^{-1}), ZnPc/SNV (equivalent ZnPc: 5 μg mL^{-1}), ZnPc-DOX/SNV (equivalent DOX: 2.5 μg mL^{-1}; ZnPc: 2.5 μg mL^{-1}) and pristine SNV (500 μg mL^{-1}), respectively. After a further incubation of 24 h, the cells were washed with PBS 3 times. One plate was irradiated with a simulated sunlight source (optical filter: 650 ± 5 nm; power density: 10 mW cm^{-2}) for 30 min and another was kept in the dark outside the incubator. The colorimetric MTT was used to determine the cell viability.

In vivo chemotherapy-PDT

Male Balb/c mice (Balb/c-nu, ~25 g) were purchased from the Academy of Military Medical Science and used under protocols approved by the 302th Military Hospital Animal Research Center. 2×10^6 HepG2 cells suspended in 200 μL phosphate buffered saline (PBS) were subcutaneously injected into the hind flank of each male Balb/c mouse. The mice bearing HepG2 tumors were treated when the tumor volume reached ~40 mm^3. The mice were randomized into seven groups (8 animals per group) for the following treatments: (group i) 100 μL of saline injected intravenously, with irradiation at 36 J cm^{-2}; (group ii) 100 μL of ZnPc (25 μg) injected intravenously, with irradiation at 36 J cm^{-2}; (group iii) 100 μL of ZnPc(5.3%)/SNV (equivalent 25 μg ZnPc) injected intravenously, with irradiation at 36 J cm^{-2}; (group iv) 100 μL of DOX (25 μg) injected intravenously, without irradiation; (group v) 100 μL of DOX/SNV (equivalent 25 μg DOX) injected intravenously, without irradiation; (group vi) 100 μL of ZnPc-DOX/PVP-Br (equivalent 12.5 μg ZnPc and 12.5 μg DOX) injected intravenously, with irradiation at 36 J cm^{-2}; (group vii) 100 μL of ZnPc-DOX/SNV (equivalent 12.5 μg ZnPc and 12.5 μg DOX) injected intravenously, with irradiation at 36 J cm^{-2}. Mice undergoing the PDT were irradiated with a simulated sunlight source (optical filter: 650 ± 5 nm; power density: 20 mW cm^{-2}) for 30 min (*i.e.*, an optical fluence rate of 36 J cm^{-2}). The tumor size was measured by a caliper every day and the volume was calculated using the equation: volume = (tumor length) × (tumor width)^2 × 0.5.[32] The relative tumor volume was calculated as V/V_0 (V, V_0 are the tumor volume measured at time t and t_0, respectively).

Results and discussion

Structural and morphological characterizations

A copolymer was designed and synthesized with a targeting capability toward HepG2 cells *via* a three-step procedure: (1) the atom transfer radical polymerization (ATRP) of *N*-vinylpyrrolidone (NVP) to obtain poly(*N*-vinylpyrrolidone) (PVP-Br), (2) the ATRP of *tert*-butyl acrylate initiated by macroinitiator PVP-Br and the subsequent deprotection of *tert*-butyl groups to produce the block copolymer PVP-*b*-PAA, and (3) the covalent grafting of folic acid (FA) onto PVP-*b*-PAA to achieve the final hydrophilic copolymer PVP-*b*-PAA-*g*-FA. The detailed synthetic process is described in the ESI (Scheme S1†). NMR spectra demonstrate the successful synthesis of PVP-Br, PVP-*b*-PAA and PVP-*b*-PAA-*g*-FA (Fig. S1–S4; Table S1†). Subsequently, a ZnPc(*x*%)/SNV solution and ZnPc-DOX/SNV colloidal materials were prepared *via* a facile microemulsion method as described in the experimental section (Fig. S5†). The design of the copolymer PVP-*b*-PAA-*g*-FA with a targeting ligand (FA) is essential for the fabrication of ZnPc-DOX/SNV micelles: the acidic DOX neutralizes the partially ionized FA to constitute the interior core of the micelle and the remaining ionized FA and terminal PVP form the exterior shell. The interaction between ZnPc and PVP was demonstrated using isothermal titration calorimetry (ITC) (Fig. 1A and S6†). The negative values of ΔH and ΔS reveal the formation of hydrogen bonding between PVP and ZnPc. The copolymer successfully loads the PDT photosensitizer (ZnPc) and chemotherapy drug (DOX) simultaneously, ensuring the implementation of the chemotherapy-PDT targeted cancer therapy.

Since monomeric ZnPc is crucial for PDT, UV-vis spectroscopy was used to study the existence state of ZnPc in the ZnPc-DOX/SNV micelle. The aqueous solution of ZnPc prefers to exist as H-type aggregates with the absorption maximum at 635 nm, but it moves to 675 nm in 60% ethanol solution (Fig. 1B). The red-shift of the ZnPc Q-band indicates the collapse of the H-type aggregation and the presence of a monomeric state in low polarity media.[49] In the case of the ZnPc(5.3%)/SNV aqueous suspension, a strong monomeric absorption at 682 nm is observed (Fig. 1B and S7A†), suggesting that the PVP-*b*-PAA-*g*-FA micelle provides a low polarity microenvironment for the existence of monomeric ZnPc. For the ZnPc-DOX/SNV sample, an insignificant red-shift in the monomeric absorbance is observed with the same intensity as that of ZnPc(5.3%)/SNV, indicating that the coexistence of DOX imposes no obvious influence on the monodispersity of ZnPc. Fig. 1C shows the fluorescence emission spectra of the above samples. The spectrum of ZnPc display a rather weak peak at 682 nm in aqueous solution, while there is a largely-enhanced emission at 692 nm in 60% ethanol solution. For the samples of ZnPc(5.3%)/SNV and ZnPc-DOX/SNV, a moderate photoluminescence intensity is observed, accompanied by a red-shift of the emission maximum to 702 and 700 nm respectively, implying their potential

Open Access Article. Published on 22 Juni 2015. Downloaded on 28.01.2026 20:20:08.
This article is licensed under a Creative Commons Attribution-NonCommercial 3.0 Unported Licence.

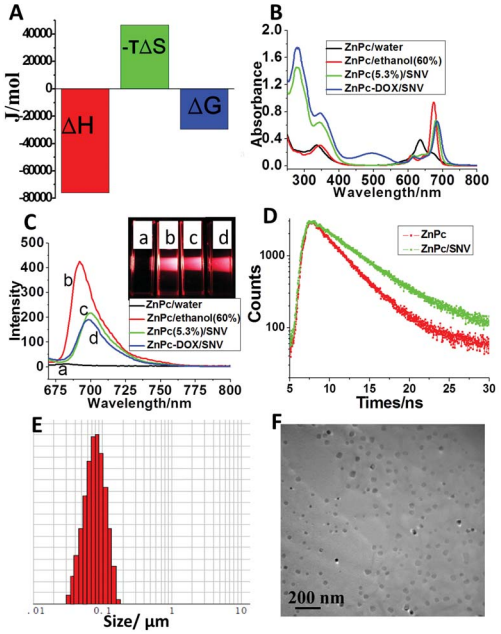

Fig. 1 (A) ITC titration measurements of PVP-Br (1.0×10^{-4} mol L^{-1}) and ZnPc (1.0×10^{-3} mol L^{-1}): the thermodynamic parameters of the interaction. (B) UV-vis absorption spectra of: pristine ZnPc (20 μg mL^{-1}) in aqueous solution, pristine ZnPc (20 μg mL^{-1}) in 60% ethanol solution, ZnPc(5.3%)/SNV and ZnPc-DOX/SNV (ZnPc equivalent to 20 μg mL^{-1}) aqueous suspension. (C) Photoluminescence spectra and photographs (inset) of: (a) ZnPc in aqueous solution, (b) ZnPc in 60% ethanol, (c) ZnPc(5.3%)/SNV, (d) ZnPc-DOX/SNV suspension. (D) Typical fluorescence decay curves of ZnPc and ZnPc/SNV. (E) The particle size distribution of ZnPc-DOX/SNV determined using a Malvern Mastersizer 2000 laser particle size analyzer. (F) TEM image of the ZnPc-DOX/SNV sample.

application in NIR fluorescence imaging. The visual results are shown in the inset of Fig. 1C. We further determined the fluorescence lifetime of ZnPc and ZnPc/SNV (Fig. 1D). Compared with the lifetime of ZnPc (3.47 ns) in aqueous solution, the fluorescence lifetime of ZnPc/SNV (5.19 ns) increased markedly, demonstrating the disaggregation of ZnPc in SNV. The equivalent hydrodynamic diameter of ZnPc-DOX/SNV in aqueous solution was determined to be ~70 nm (Fig. 1E) using the dynamic light scattering (DLS) measurements. Transmission electron microscopy (TEM) images clearly show the formation of spherical micelles with a diameter range of 20–60 nm (Fig. 1F and S8†). The zeta potential of the ZnPc-DOX/SNV suspension was determined to be −11.1 mV (Fig. S9†). The surface charge of the micelle facilitates its stable dispersion in aqueous solution for as long as 7 days.

Measurements of singlet oxygen

The singlet oxygen production efficiency of ZnPc(*x*%)/SNV is the key factor of the PDT performance. The generation of singlet oxygen by ZnPc(*x*%)/SNV was chemically detected using the disodium salt of 9,10-anthracenedipropionic acid (ADPA), whose absorption band at 378 nm as a detector can be bleached to its nonfluorescent endoperoxide in the presence of $^1O_2$.[48] Fig. 2 and S10† show the absorption spectra of ADPA at 378 nm with the presence of various samples as a function of irradiation time under 650 nm light. For the ADPA solution alone, no change in the absorbance was observed under light irradiation (Fig. S10A†). The addition of pristine ZnPc into the ADPA solution accelerates the absorbance decrease to some extent (Fig. 2A), indicating the generation of singlet oxygen by ZnPc. In the case of the ZnPc(*x*%)/SNV materials (*x*% ranges between 14.3–5.3%), a sharp decrease in absorbance is observed with an irradiation time of 6 min (Fig. 2B, S10B and C†). It was found that the sample of ZnPc(5.3%)/SNV exhibits the strongest capability to produce singlet oxygen, in good accordance with its strongest monomeric absorbance (Fig. S7†). After an irradiation time of 6 min, a decrease of 93.2% in the absorbance of the ADPA probe is observed for ZnPc(5.3%)/SNV; while only a 15.3% decrease is found for pristine ZnPc. It is therefore concluded that the monomeric state of ZnPc encapsulated in the PVP-*b*-PAA-*g*-FA micelle plays a key role in boosting the production of singlet oxygen. The singlet oxygen production efficiency of ZnPc-DOX/SNV was also investigated, which displays a rather close value to that of ZnPc(5.3%)/SNV (Fig. 2C and D). This indicates that the coexistence of DOX does not affect the singlet oxygen production of ZnPc. In addition, the release tests indicate that the absorbance of ZnPc-DOX/SNV at 682 nm (originating from ZnPc) remains unchanged while the one at 495 nm (originating from DOX) decreased by 25% after 48 h dialysis (Fig. S11†), indicating the effectiveness of the delivery system.

In vitro anticancer activity

The anticancer activity of ZnPc-DOX/SNV was studied by *in vitro* tests performed with HepG2 cells. HepG2 cells were incubated separately with DOX, ZnPc, ZnPc/PVP-Br, DOX/SNV, ZnPc/SNV, ZnPc-DOX/PVP-Br and ZnPc-DOX/SNV with concentrations ranging from 0 to 10 μg mL^{-1} for 24 h, and then washed with PBS three times. Subsequently, the cells were irradiated with

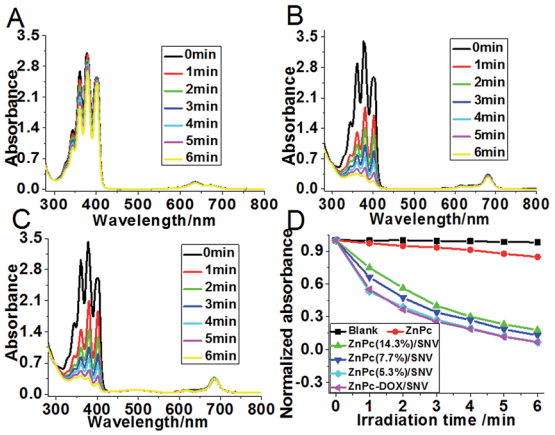

Fig. 2 Decay curves of the ADPA absorbance in the presence of (A) ZnPc, (B) ZnPc(5.3%)/SNV and (C) ZnPc-DOX/SNV as a function of irradiation time (at 650 nm). (D) The normalized decay curves of the ADPA absorbance at 378 nm as a function of irradiation time, in the presence of pristine ZnPc, ZnPc(*x*%)/SNV, ZnPc-DOX/SNV as well as the blank measurement.

This journal is © The Royal Society of Chemistry 2015

Open Access Article. Published on 22 Juni 2015. Downloaded on 28.01.2026 20:20:08.
This article is licensed under a Creative Commons Attribution-NonCommercial 3.0 Unported Licence.

NIR light (650 nm) at a power density of 10 mW cm^{-2} for 30 min. The standard methyl thiazolyl tetrazolium (MTT) assay was carried out to determine the relative cell viability. As shown in Fig. 3A and B, a significant anticancer effect occurs and enhances gradually along with the increase of dosage from 0.1 to 10 μg mL^{-1}. The half maximal inhibitory concentration (IC_{50}) of ZnPc-DOX/SNV is 0.60 μg mL^{-1}, which is smaller than that of DOX (2.29 μg mL^{-1}), DOX/SNV (3.66 μg mL^{-1}), ZnPc (37.25 μg mL^{-1}), ZnPc/SNV (1.71 μg mL^{-1}) and ZnPc-DOX/PVP-Br (3.91 μg mL^{-1}). The results absolutely verify the synergistic effect of chemotherapy and PDT to achieve a greatly enhanced anticancer activity. Compared with the results for treatment with ZnPc-DOX/PVP-Br and ZnPc-DOX/SNV, the anticancer efficacy was highly enhanced *via* conjugation with FA, demonstrating the effectiveness of FA toward specifically targeting HepG2 cells. In order to visualize the anticancer results, HepG2 cells were stained with propidium iodide (PI), which is excluded by viable cells but can penetrate into the cell membrane of dead cells.[34] The HepG2 cells treated with 5 μg mL^{-1} of ZnPc, ZnPc(5.3%)/PVP-Br, ZnPc(5.3%)/SNV under irradiation are displayed in Fig. 3C–F.

The anticancer activity of DOX, DOX/SNV, ZnPc-DOX/PVP-Br and ZnPc-DOX/SNV is shown in Fig. 3G–J. The results verify that the ZnPc-DOX/SNV drug displays superior anticancer efficacy, in accordance with the *in vitro* tests above (Fig. 3A and B). For comparison, the phototoxicities were also studied through incubating HepG2 cells in these media (Fig. S12†). DOX shows a strong cytotoxicity without PDT performance; while some cytotoxicity as well as rather poor PDT effectiveness are observed for ZnPc alone. For the sample of ZnPc/SNV, the cytotoxicity of ZnPc is significantly depressed by encapsulation into the copolymer and the sample displays a better PDT performance owing to the targeting of FA toward the HepG2 cells. In the case of the ZnPc-DOX/SNV drug which combines chemotherapy and PDT, the cell viabilities are found to be 0.56 (no irradiation) and 0.07 (irradiation), demonstrating its largely-enhanced anticancer activity by virtue of the chemotherapy-PDT. Moreover, in order to provide distinct evidence of the synergistic effect of PDT and chemotherapy, the intracellular ROS signal was examined by using a fluorescent probe, dichlorofluorescein diacetate (DCFH-DA). As shown in Fig. S13,† the sample of HepG2 cells treated with ZnPc-DOX/SNV displays the strongest fluorescence intensity compared with the control groups, which indicates that ZnPc-DOX/SNV induces the highest ROS production with HepG2 cells. In addition, the HepG2 cell sample treated with ZnPc-DOX/SNV also shows the most significant apoptosis (Fig. S14†).

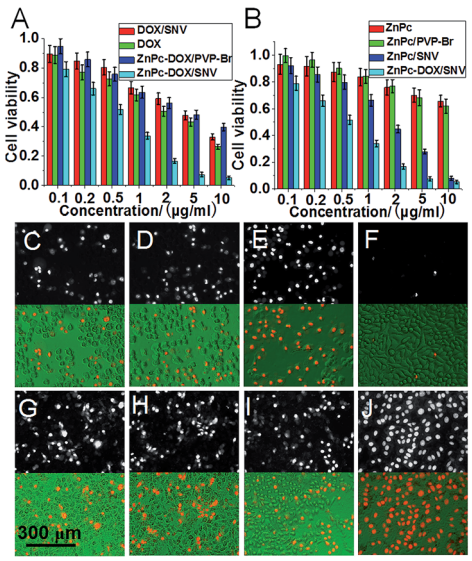

Fig. 3 The antitumor performance of (A) DOX/SNV, DOX, ZnPc-DOX/PVP-Br, ZnPc-DOX/SNV, (B) ZnPc, ZnPc/PVP-Br, ZnPc/SNV, ZnPc-DOX/SNV, with a concentration in the range 0–10 μg mL^{-1} after 24 h incubation and 0.5 h irradiation. Fluorescence microscopy and merged images of the HepG2 cells treated with various samples and irradiation (5 μg mL^{-1} and 24 h incubation): (C) ZnPc, (D) ZnPc(5.3%)/PVP-Br, (E) ZnPc(5.3%)/SNV, (F) blank, (G) DOX, (H) DOX/SNV, (I) ZnPc-DOX/PVP-Br, (J) ZnPc-DOX/SNV.

Fluorescence imaging and *in vivo* antitumor assay

To investigate the feasibility and targeting ability of ZnPc-DOX/SNV for *in vivo* fluorescence imaging and theranostics, 100 μL of ZnPc-DOX/SNV or ZnPc-DOX/PVP-Br (equivalent 25 μg ZnPc and 25 μg DOX) was injected intravenously into the tails of the mice, and fluorescence images were recorded on a Carestream Molecular Imaging *In vivo* MS FX PRO system. As shown in Fig. 4A, the fluorescence signal from the tumor (at the hind flank of the mouse; Fig. S15†) becomes strongest at 24 h after the intravenous injection, which is related to the following two simultaneous processes: drug circulation/metabolization in the whole body and gradual accumulation at the tumor site. The results demonstrate a good targeting ability of ZnPc-DOX/SNV in the mice. In the control sample of ZnPc-DOX/PVP-Br, no obvious fluorescence signal from the tumor at the same position is observed during the whole metabolic process after the intravenous injection (Fig. 4B). The results show that ZnPc-DOX/SNV can be used as a good NIR agent for *in vivo* targeted imaging. Finally, the *in vivo* therapeutic efficacy of the ZnPc-DOX/SNV induced tumor treatment was studied. Seven groups of HepG2 tumor-bearing mice (8 mice per group) were employed in this work. For the target group, tumors were intravenously injected with ZnPc-DOX/SNV (dosage: both ZnPc and DOX were 0.5 mg kg^{-1}) and irradiated by a simulated sunlight source (optical filter: 650 ± 5 nm) with a power density of 20 mW cm^{-2} for 30 min (fluence rate: 36 J cm^{-2}). Other control groups consisted of mice given a saline injection with irradiation, ZnPc injection with irradiation, ZnPc/SNV injection with irradiation, DOX injection without irradiation, DOX/SNV injection without irradiation, ZnPc-DOX/PVP-Br injection with irradiation (the total drug dosage: 1 mg kg^{-1}). The tumor size was measured using a caliper each day after the treatment. As shown in Fig. 4C, the *in vivo* antitumor efficiency increases in the following order: saline < DOX ≈ ZnPc ≈ ZnPc-DOX/PVP-Br < DOX/SNV < ZnPc/SNV < ZnPc-DOX/SNV. The ZnPc-DOX/SNV drug exhibits the most superior *in vivo* antitumor performance, *i.e.*, the growth speed of the tumor was restrained to a great extent in comparison with the control groups, and the tumor

Open Access Article. Published on 22 Juni 2015. Downloaded on 28.01.2026 20:20:08.
This article is licensed under a Creative Commons Attribution-NonCommercial 3.0 Unported Licence.

almost disappeared by the fourth day. This striking contrast can be further observed in the mice photographs after treatment for 14 days (Fig. 4D). In marked contrast, both the tumors in the ZnPc/SNV and DOX/SNV control groups show a faster growth speed, illustrating the combined chemotherapy-PDT leads to a significantly enhanced therapeutic efficacy. In addition, haematoxylin and eosin (H&E) staining of tumor slices was also carried out and collected one day after the treatment for all of the seven groups (Fig. 4E). As expected, significant cancer cell damage was noticed in the tumor with the ZnPc-DOX/SNV injection and irradiation (Fig. 4E, E7); while only partial necrosis/apoptosis can be observed in the other six control groups. The results are consistent with the growth tendency of the tumor (Fig. 4C and D). These results clearly demonstrate that ZnPc-DOX/SNV can serve as a powerful chemotherapy-PDT agent for *in vivo* antitumor treatment, with an ultra-low dosage of 1.0 mg kg^{-1} and an optical fluence rate of 36 J cm^{-2}. The excellent *in vivo* antitumor performance of ZnPc-DOX/SNV with good biocompatibility demonstrates great promise for its employment in targeted tumor therapy.

Structure–property correlations

The excellent chemotherapy-PDT systematic therapy can be attributed to the following three factors. Firstly, the grafted FA molecule in the copolymer provides the targeting ability which increases the drug intake by the HepG2 cells. Fig. 5A shows that the fluorescence intensity of ZnPc-DOX/SNV (with the presence of FA) in the cell lysate sample is a lot stronger than that of ZnPc-DOX/PVP-Br (without FA) from 1 to 10 μg mL^{-1}, which verifies the over-expression of FA toward the HepG2 cells. We further investigated the intake of ZnPc-DOX/SNV and ZnPc-DOX/PVP-Br using fluorescence microscopy. HepG2 cells were respectively incubated with ZnPc-DOX/SNV and ZnPc-DOX/PVP-Br with a concentration of 5 μg mL^{-1} for 24 h, and their fluorescence images were recorded. As shown in Fig. 5B, the fluorescence intensity of HepG2 cells incubated with the former (B1) is obviously stronger than with the latter (B2), further demonstrating the larger intake of ZnPc-DOX/SNV owing to the presence of the chemically-modified FA target.

Secondly, the hydrogen bonding interaction between PVP and ZnPc facilitates the monomeric state of ZnPc in the SNV, which tremendously enhances the PDT performance of ZnPc (Fig. 6A). When the ZnPc molecule exists in a monomeric state, its electron can be easily excited to the first short-lived singlet state when irradiated with NIR light, followed by an intersystem crossing to a longer-lived triplet state.[13] Subsequently, the ZnPc triplet state transfers energy to ground-state triplet oxygen to produce $^1O_2$. In contrast, the π–π interaction of the ZnPc molecules in aggregates leads to a self-quenching effect of the excited state,[41] which decreases the production of $^1O_2$. Therefore, the monomeric ZnPc within the SNV as a result of drug–support interactions is crucial for the PDT performance.

Thirdly, this systematic chemotherapy-PDT not only overcomes the shortcomings of individual anticancer therapies, but also imposes a significant synergistic therapeutic efficacy compared with individual methods. It has been reported that dual-modal treatment strategies can achieve an enhanced synergistic therapeutic effect.[10,11,50] In this work, the synergistic effect of a combined chemotherapy-PDT was also demonstrated. As revealed by the fluorescence imaging study (Fig. 3E and 5C), PDT leads to an obvious treatment effect while chemotherapy only shows a weak performance. However, HepG2 cells treated with chemotherapy undergo an inflammatory response (*e.g.*, a morphology change and a decrease in cell activity); the assistance of PDT would easily cause the final death

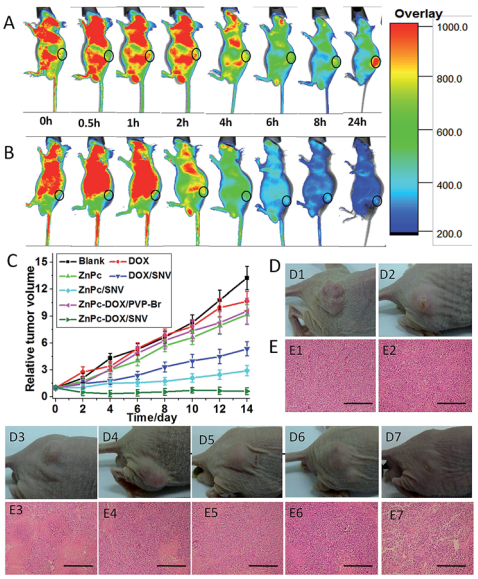

Fig. 4 *In vivo* fluorescence imaging of mice after intravenous injection with 100 μL of (A) ZnPc-DOX/SNV and (B) ZnPc-DOX/PVP-Br at different time points (0 h, 0.5 h, 1 h, 2 h, 4 h, 6 h, 8 h, 24 h). (C) Tumor growth curves of the seven groups of mice after treatment. The tumor volume was normalized to the initial size; the error bar is based on the standard deviation from the mice in each group. (D) Representative photos of mice bearing a HepG2 tumor after various treatments for 14 days (D1: saline, irradiation at 36 J cm^{-2}; D2: ZnPc, irradiation at 36 J cm^{-2}; D3: ZnPc/SNV, irradiation at 36 J cm^{-2}; D4: DOX, no irradiation; D5: DOX/SNV, no irradiation; D6: ZnPc-DOX/PVP-Br, irradiation at 36 J cm^{-2}; D7: ZnPc-DOX/SNV, irradiation at 36 J cm^{-2}). (E) H&E stained tumor slices collected from the seven groups after 48 h of various treatments (E1–E7: the same as D; the scale bar is 300 μm).

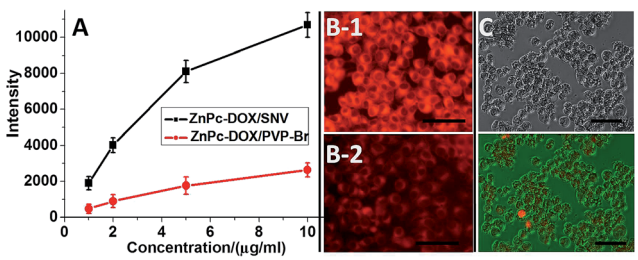

Fig. 5 (A) Fluorescence intensities of cell lysate samples from HepG2 cells incubated with various concentrations of ZnPc-DOX/SNV and ZnPc-DOX/PVP-Br. (B1 and B2) Fluorescence images of HepG2 cells incubated with 5 μg mL^{-1} of ZnPc-DOX/SNV and ZnPc-DOX/PVP-Br, respectively. (C) Bright field microscopy image and a merged image of HepG2 cells treated with ZnPc-DOX/SNV without irradiation (5 μg mL^{-1}, 24 h incubation; HepG2 cells were stained with PI). The scale bar is 100 μm in (B) and (C).

This journal is © The Royal Society of Chemistry 2015

Open Access Article. Published on 22 Juni 2015. Downloaded on 28.01.2026 20:20:08.
This article is licensed under a Creative Commons Attribution-NonCommercial 3.0 Unported Licence.

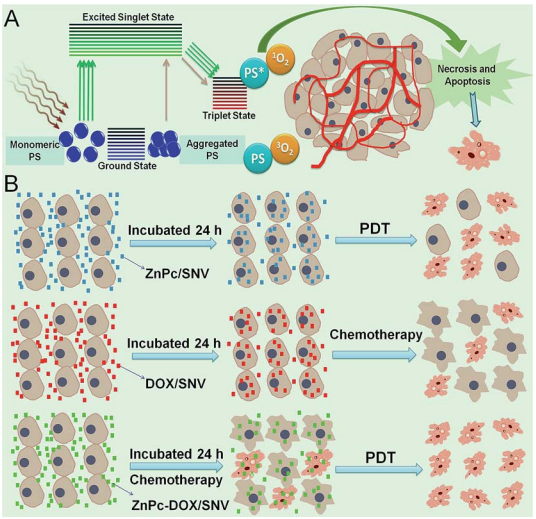

Fig. 6 A schematic representation of enhanced PDT and the synergistic effect in chemo-PDT therapy: (A) the mechanism of action of photodynamic therapy. (B) A schematic representation of the synergistic effect in this chemo-PDT therapy.

of HepG2 cells, accounting for the largely enhanced therapy. This is schematically illustrated in Fig. 6B. Therefore, the ingenious design, synthesis and assembly of structure units are key factors for the excellent therapeutic effect.

Conclusions

In summary, a supramolecular nanovehicle (SNV) toward systematic and targeted chemotherapy-PDT tumor therapy was fabricated through incorporation of ZnPc and DOX into a copolymer (PVP-*b*-PAA-*g*-FA). Acidic DOX neutralizes partially ionized FA to constitute the hydrophobic core and the hydrophilic ionized FA and terminal PVP are exposed at the exterior shell, endowing the formation of a stable SNV. The dispersion of the ZnPc photosensitizer in a monomeric state was obtained in this system, which shows a NIR photoactivity and high singlet oxygen production efficiency.

In vitro tests performed with HepG2 cells reveal that ZnPc-DOX/SNV exhibits a satisfactory anticancer effectiveness (equivalent tests with 2.5 μg mL^{-1} ZnPc and 2.5 μg mL^{-1} DOX result in 92.7% cell death), good biocompatibility as well as low cytotoxicity. *In vivo* studies using mice with intravenous injections demonstrate an excellent antitumor behavior, with an ultra-low drug dose of 1 mg kg^{-1} (the summation of ZnPc and DOX) and a low optical fluence rate of 36 J cm^{-2}, by virtue of the synergistic effect of chemotherapy and PDT. In addition, NIR fluorescence imaging measurements substantiate its applications for *in vivo* detection and imaging. Therefore, the supramolecular nanovehicle (SNV) fabricated in this work holds a great promise in the field of targeted tumor imaging and therapy.

Acknowledgements

This work was supported by the 973 Program (Grant No. 2014CB932104), the National Natural Science Foundation of China (NSFC) and the Specialized Research Fund for the Doctoral Program of Higher Education (20130010110013). M. W. appreciates the China National Funds for Distinguished Young Scholars of the NSFC. D. Y. thanks the China National Funds for Excellent Young Scholars of the NSFC. We are thankful for the helpful discussions with Dr Jiaoyang Luo and Prof. Meihua Yang from the Institute of Medicinal Plant Development, the Chinese Academy of Medical Sciences and the Peking Union Medical College.

Notes and references

1 W. Wu, R. Li, X. Bian, Z. Zhu, D. Ding, X. Li, Z. Jia, X. Jiang and Y. Hu, *ACS Nano*, 2009, **3**, 2740.
2 J. Wang, X. Wang, Y. Song, J. Wang, C. Zhang, C. Chang, J. Yan, L. Qiu, M. Wu and Z. Guo, *Chem. Sci.*, 2013, **4**, 2605.
3 K. Yang, H. Xu, L. Cheng, C. Sun, J. Wang and Z. Liu, *Adv. Mater.*, 2012, **24**, 5586.
4 K. Liu, Y. Liu, Y. Yao, H. Yuan, S. Wang, Z. Wang and X. Zhang, *Angew. Chem., Int. Ed.*, 2013, **52**, 8285.
5 W.-S. Kuo, C.-N. Chang, Y.-T. Chang, M.-H. Yang, Y.-H. Chien, S.-J. Chen and C.-S. Yeh, *Angew. Chem., Int. Ed.*, 2010, **49**, 2711.
6 M. R. Reithofer, K. H. Chan, A. Lakshmanan, D. H. Lam, A. Mishra, B. Gopalan, M. Joshi, S. Wang and C. A. E. Hauser, *Chem. Sci.*, 2014, **5**, 625.
7 D. Lane, *Nat. Biotechnol.*, 2006, **24**, 163.
8 W. Fan, B. Shen, W. Bu, F. Chen, K. Zhao, S. Zhang, L. Zhou, W. Peng, Q. Xiao, H. Xing, J. Liu, D. Ni, Q. He and J. Shi, *J. Am. Chem. Soc.*, 2013, **135**, 6494.
9 S. Sengupta, D. Eavarone, I. Capila, G. Zhao, N. Watson, T. Kiziltepe and R. Sasisekharan, *Nature*, 2005, **436**, 568.
10 W. Fan, B. Shen, W. Bu, X. Zheng, Q. He, Z. Cui, K. Zhao, S. Zhang and J. Shi, *Chem. Sci.*, 2015, **6**, 1747.
11 T. M. Sun, J. Z. Du, Y. D. Yao, C. Q. Mao, S. Dou, S. Y. Huang, P. Z. Zhang, K. W. Leong, E. W. Song and J. Wang, *ACS Nano*, 2011, **5**, 1483.
12 D. Dolmans and R. D. Fukumura, *Nat. Rev. Cancer*, 2003, **3**, 380.
13 A. Castano, P. Mroz and M. Hamblin, *Nat. Rev. Cancer*, 2006, **6**, 535.
14 Z. Chen, Z. Li, J. Wang, E. Ju, L. Zhou, J. Ren and X. Qu, *Adv. Funct. Mater.*, 2014, **24**, 522.
15 M. J. Sailor and J. H. Park, *Adv. Mater.*, 2012, **24**, 3779.
16 S. H. C. Askes, A. Bahreman and S. Bonnet, *Angew. Chem., Int. Ed.*, 2014, **53**, 1029.
17 R. Liang, R. Tian, L. Ma, L. Zhang, Y. Hu, J. Wang, M. Wei, D. Yan, D. G. Evans and X. Duan, *Adv. Funct. Mater.*, 2014, **24**, 3144.
18 C. Mari, V. Pierroz, S. Ferrari and G. Gasser, *Chem. Sci.*, 2015, **6**, 2660.
19 P. Rai, S. Mallidi, X. Zheng, R. Rahmanzadeh, Y. Mir, S. Elrington, A. Khurshid and T. Hasan, *Adv. Drug Delivery Rev.*, 2010, **62**, 1094.
20 J. P. Celli, B. Q. Spring, I. Rizvi, C. L. Evans, K. S. Samkoe, S. Verma, B. W. Pogue and T. Hasan, *Chem. Rev.*, 2010, **110**, 2795.

Open Access Article. Published on 22 Juni 2015. Downloaded on 28.01.2026 20:20:08.
This article is licensed under a Creative Commons Attribution-NonCommercial 3.0 Unported Licence.

21 K. Lang, J. Mosinger and D. M. Wagnerová, *Coord. Chem. Rev.*, 2004, **248**, 321.
22 A. E. O'Connor, W. M. Gallagher and A. T. Byrne, *Photochem. Photobiol.*, 2009, **85**, 1053.
23 W. Liu, T. J. Jensen, F. R. Fronczek, R. P. Hammer, K. M. Smith and M. G. H. Vicente, *J. Med. Chem.*, 2005, **48**, 1033.
24 K. Hayashi, M. Nakamura, H. Miki, S. Ozaki, M. Abe, T. Matsumoto, T. Kori and K. Ishimura, *Adv. Funct. Mater.*, 2014, **24**, 503.
25 B. A. Bench, A. Beveridge, W. M. Sharman, G. J. Diebold, J. E. Lier and S. M. Gorun, *Angew. Chem., Int. Ed.*, 2002, **41**, 748.
26 S. Kim, T. Ohulchanskyy, H. Pudavar, R. Pandey and P. Prasad, *J. Am. Chem. Soc.*, 2007, **129**, 2669.
27 H. K. Yoon, X. Lou, Y.-C. Chen, Y.-E. K. Lee, E. Yoon and R. Kopelman, *Chem. Mater.*, 2014, **26**, 1592.
28 M. Velusamy, J. Y. Shen, J. T. Lin, Y. C. Lin, C. C. Hsieh, C. H. Lai, C. W. Lai, M. L. Ho, Y. C. Chen and P. T. Chou, *Adv. Funct. Mater.*, 2009, **19**, 2388.
29 X. Zheng, X. Wang, H. Mao, W. Wu, B. Liu and X. Jiang, *Nat. Commun.*, 2015, **6**, 5834.
30 X. Wu, M. Yu, B. Lin, H. Xing, J. Han and S. Han, *Chem. Sci.*, 2015, **6**, 798.
31 C. Xing, L. Liu, H. Tang, X. Feng, Q. Yang, S. Wang and G. C. Bazan, *Adv. Funct. Mater.*, 2011, **21**, 4058.
32 M. Mitsunaga, M. Ogawa, N. Kosaka, L. T. Rosenblum, P. L. Choyke and H. Kobayashi, *Nat. Med.*, 2011, **17**, 1685.
33 S.-J. Yang, F.-H. Lin, H.-M. Tsai, C.-F. Lin, H.-C. Chin, J.-M. Wong and M.-J. Shieh, *Biomaterials*, 2011, **32**, 2174.
34 M. Brasch, A. Escosura, Y. Ma, C. Uetrecht, A. J. R. Heck, T. Torres and J. J. L. M. Cornelissen, *J. Am. Chem. Soc.*, 2011, **133**, 6878.
35 N. Nishiyama, Y. Morimoto, W. D. Jang and K. Kataoka, *Adv. Drug Delivery Rev.*, 2009, **61**, 327.
36 S. Lee, J. H. Ryu, K. Park, A. Lee, S. Y. Lee, I. C. Youn, C. H. Ahn, S. M. Yoon, S. J. Myung, D. H. Moon, X. Chen, K. Choi, I. C. Kwon and K. Kim, *Nano Lett.*, 2009, **9**, 4412.
37 M. Steiner, I. Hartmann, E. Perrino, G. Casi, S. Brighton, I. Jelesarov, G. J. L. Bernardes and D. Neri, *Chem. Sci.*, 2013, **4**, 297.
38 L. Gao, J. Fei, J. Zhao, H. Li, Y. Cui and J. Li, *ACS Nano*, 2012, **6**, 8030.
39 U. Basu, I. Khan, A. Hussain, P. Kondaiah and A. R. Chakravarty, *Angew. Chem., Int. Ed.*, 2012, **51**, 2658.
40 C. Wang, L. Cheng, Y. Liu, X. Wang, X. Ma, Z. Deng, Y. Li and Z. Liu, *Adv. Funct. Mater.*, 2013, **23**, 3077.
41 K. J. Son, H.-J. Yoon, J.-H. Kim, W.-D. Jang, Y. Lee and W.-G. Koh, *Angew. Chem., Int. Ed.*, 2011, **50**, 11968.
42 G. Bonadonna, L. Gianni, A. Santoro, V. Bonfante, P. Bidoli, P. Casali, R. Demicheli and P. Valagussa, *Ann. Oncol.*, 1993, **4**, 359.
43 W.-P. Li, P.-Y. Liao, C.-H. Su and C.-S. Yeh, *J. Am. Chem. Soc.*, 2014, **136**, 10062.
44 H. Zhou, P. Jiao, L. Yang, X. Li and B. Yan, *J. Am. Chem. Soc.*, 2011, **133**, 680.
45 B. Liang, M.-L. He, C. Chan, Y. Chen, X.-P. Li, Y. Li, D. Zheng, M. C. Lin, H.-F. Kung, X.-T. Shuai and Y. Peng, *Biomaterials*, 2009, **30**, 4014.
46 A. Chango, A. Nour, S. Bousserouel, D. Eveillard, P. M. Anton and J.-L. Guéant, *J. Nutr. Biochem.*, 2009, **20**, 312.
47 R. W. Hay, G. A. Lawrance and N. F. Curtis, *J. Chem. Soc., Perkin Trans.*, 1975, **1**, 591.
48 G. Obaid, I. Chambrier, M. J. Cook and D. A. Russell, *Angew. Chem., Int. Ed.*, 2012, **51**, 6158.
49 K. M. Kadish, K. M. Smith and R. Guilard, *Handbook of Porphyrin Science*, World Scientific, Singapore, 2010.
50 B. Tian, C. Wang, S. Zhang, L. Feng and Z. Liu, *ACS Nano*, 2011, **5**, 7000.

This journal is © The Royal Society of Chemistry 2015